Mechanisms of Ageing and Development 230 (2026) 112159

Contents lists available at ScienceDirect

Mechanisms of Ageing and Development

journal homepage: www.elsevier.com/locate/mechagedev

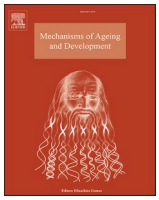

Vitisin B rejuvenates senescence via *WBP2NL* regulation

Jee Hee Yoon [a,1], Yun Haeng Lee [a,1], Sekyung Oh [b,1], Kyeong Seon Lee [c,d], Ji Ho Park [a], Yoo Jin Lee [a], Byeonghyeon So [a], Duyeol Kim [a], Minseon Kim [a], Hyung Wook Kwon [a,e], Youngjoo Byun [c,d,*,2], Ki Yong Lee [c,d,*], Joon Tae Park [a,e,**]

[a] Division of Life Sciences, College of Life Sciences and Bioengineering, Incheon National University, Incheon 22012, Republic of Korea
[b] Department of Medical Sciences, Catholic Kwandong University College of Medicine, Incheon 22711, Republic of Korea
[c] College of Pharmacy, Korea University, Sejong 30019, Republic of Korea
[d] Interdisciplinary Major Program in Innovative Pharmaceutical Sciences, Korea University, Sejong 30019, Republic of Korea
[e] Convergence Research Center for Insect Vectors, Incheon National University, Incheon 22012, Republic of Korea

ARTICLE INFO

Keywords:
ROS
Senescence rejuvenation
Vitisin B
WBP2NL

ABSTRACT

One of the main factors contributing to aging is reactive oxygen species (ROS), which are produced by dysfunctional mitochondria. Reducing ROS generation is considered an essential treatment for senescence, but no effective treatment has been developed yet. In this study, vitisin B, a tetramer of resveratrol, was found to be an efficient reagent that reduces mitochondrial ROS generation after screening phenylpropanoids (PPs), metabolites produced to overcome ROS-mediated stress in plants. Vitisin B induced mitochondrial functional recovery by activating mitophagy and removing dysfunctional mitochondria. Mitochondrial functional recovery by vitisin B decreased mitochondrial ROS, a by-product generated from dysfunctional mitochondria. In addition, ROS reduction by vitisin B restored senescence-associated phenotypes. RNA sequencing identified *WBP2 N-Terminal Like* (*WBP2NL*) as a gene essential for vitisin B-mediated senescence rejuvenation. Knockdown of *WBP2NL* exhibited effects similar to those of vitisin B, reducing mitochondrial ROS generation and consequently reversing senescence-associated phenotypes. This study elucidates a novel mechanism by which vitisin B reverses senescence by lowering mitochondrial ROS generation. This discovery opens the way to new therapeutic options to control aging by modulating mitochondrial ROS production.

1. Introduction

Both free radical species, such as superoxide anions and hydroxyl radicals are classified as reactive oxygen species (ROS) (Herb et al., 2021). ROS within physiological concentrations plays a key role in signaling and homeostasis (Herb et al., 2021). However, ROS above physiological concentrations can induce oxidative stress, potentially damaging cellular components (Afzal et al., 2023). ROS is generated by decreased efficiency of the mitochondrial electron transport chain (ETC), leaking electrons to oxygen (Zhao et al., 2019). In addition to being a major source of ROS, dysfunctional mitochondria are the organelles that are damaged by ROS (Zhao et al., 2019). Accelerated mitochondrial damage by ROS further increases mitochondrial ROS production, ultimately leading to senescence (Lee et al., 2023). Therefore, therapies targeting mitochondrial ROS production may be beneficial in rejuvenating senescence, but effective therapies have not yet been developed.

Phenylpropanoids (PPs) are secondary metabolites produced by plants to protect themselves in response to various external stimuli, including oxidative stress (Korkina, 2007). For example, resveratrol, a member of PPs, can scavenge radical species and inhibit lipid peroxidation (Fabris et al., 2008; Rossi et al., 2013). In addition, curcumin, a member of PPs, can chelate free radicals and inhibit oxidative stress (Fabris et al., 2008; Rossi et al., 2013). Recent studies found that PP has antiviral, antibacterial, and antifungal activities, suggesting numerous health benefits for humans (Neelam et al., 2020). Most of these benefits are associated with the free radical chelating activity of PPs (Neelam et al., 2020). However, whether these properties of PPs can be used to

* Corresponding authors at: College of Pharmacy, Korea University, Sejong 30019, Republic of Korea.
** Corresponding author at: Division of Life Sciences, College of Life Sciences and Bioengineering, Incheon National University, Incheon 22012, Republic of Korea.
E-mail addresses: yjbyun1@korea.ac.kr (Y. Byun), kylee11@korea.ac.kr (K.Y. Lee), joontae.park@inu.ac.kr (J.T. Park).
[1] These authors contributed equally to this work.
[2] orcid.org/0000–0002–0297–7734

https://doi.org/10.1016/j.mad.2026.112159
Received 11 June 2025; Received in revised form 16 December 2025; Accepted 20 January 2026
Available online 21 January 2026

treat aging has not yet been elucidated.

Reagents commonly used to detect mitochondrial ROS include dihydrorhodamine 123 (DHR123) and MitoSOX. DHR123 reacts with mitochondrial hydroxyl radicals and is oxidized to the cationic compound rhodamine 123, which accumulates within mitochondria, allowing the quantification of mitochondrial hydroxyl radicals (Dickinson et al., 2010). MitoSOX, a mitochondrial-targeted derivative of dihydroethidium, selectively reacts with superoxide anions in the mitochondrial matrix to form a fluorescent cationic product, thereby allowing the quantification of mitochondrial superoxide anions (Kauffman et al., 2016).

In this study, we discovered that vitisin B, a PP, restores reduces the production of ROS within mitochondria. This restoration of mitochondrial function by vitisin B resulted in the improvement of senescence-associated phenotypes. Through transcriptome analysis, we found the mechanism by which vitisin B rejuvenates senescence by regulating *WBP2NL* expression. Here, we propose that the novel mechanism could be utilized as a new therapeutic approach for aging or age-related diseases.

2. Materials and methods

2.1. Cell culture

Human dermal fibroblasts (PCS-201–010, ATCC, Manassas, VA, USA) were cultured according to previously described protocols (Yoon et al., 2024). Human dermal fibroblasts were classified as either senescent or young fibroblasts depending on whether their cell number doubled in more than 14 days or within 2 days (Cho et al., 2022; Kang et al., 2017; Yoon et al., 2018). Additionally, human dermal fibroblasts were classified as senescent or young fibroblasts depending on whether they had more than 60 % or less than 2 % of senescence-associated β-galactosidase (SA-β-gal) positive cells, respectively (Kim et al., 2023a) (Figure S1). Furthermore, in experiments measuring the growth curve, senescent fibroblasts showed a growth plateau between 8 and 16 days, which indicates the Hayflick limit (Figure S2). The senescence status of senescent fibroblasts was also analyzed using the expression of antiproliferative markers p16, p21, and p53. Compared with young fibroblasts, senescent fibroblasts showed markedly increased expression of p16, p21, and p53, confirming their antiproliferative status (Figure S3).

2.2. SA-β-gal staining

SA-β-gal staining was performed according to the manufacturer's instructions (9860, Cell Signaling Technology, Beverly, MA, USA). The percentage of SA-β-gal-positive cells relative to the total number of cells was calculated in randomly selected fields of view.

2.3. Preparation of natural compounds

Calycosin-7-O-β-D-glucoside, oxyfudanine, and vitisin B were isolated from *Astragalus membranaceus* (Vinh et al., 2023), *Angelica dahurica* (Wei and Ito, 2006) and *Vitis amurensis* (Oh et al., 2021), respectively. The structure of the natural compound was analyzed by ^{1}H– and ^{13}C–NMR. The supplemental information (Figures S4–S9) contains the analysis data.

2.4. Analysis of reactive oxygen species (ROS) using flow cytometry

Senescent fibroblasts were treated with DMSO (0.01 %) and 4 μM natural substances (calycosine-7-O-β-D-glucoside, oxyfudanine, and vitisin B) at 4-day intervals for 12 days. The cells were next treated for 30 min at 37°C in medium that contained either 30 μM DHR123 (10056–1, Biotium, Fremont, CA, USA) or 5 μM MitoSOX (M3600, Life Technologies, Carlsbad, CA, USA). ROS were evaluated in accordance with the recommendations of a previous study (Yoon, Kim et al., 2024).

Table 1
Details of antibodies for Western blots.

Antibody	Catalogue number	Dilution
p16 antibody	sc-1661, Santa Cruz Biotechnology, Dallas, TX, USA	1:200
p21 antibody	sc-6246, Santa Cruz Biotechnology	1:200
p53 antibody	A19585, Abclonal, Boston, MA, USA	1:200
LC3B antibody	A19665, Abclonal	1:200
phospho-ATM antibody	S1981, ab81292, Abcam, Waltham, MA, USA	1:200
p62 antibody	5114, Cell Signaling Technology	1:200
β-actin antibody	sc-47778, Santa Cruz Biotechnology	1:1000
horseradish peroxidase (HRP)-conjugated secondary antibody	1706515, Bio-Rad, Hercules, CA, USA	1:1000
HRP-conjugated secondary antibody	1706516, Bio-Rad	1:1000

2.5. Cell proliferation assay

For 12 days, senescent fibroblasts were treated with vitisin B at concentrations ranging from 0 to 4 μM at 4-day intervals. Cell proliferation was measured using the EZ-cytox reagent (EZ-500, DoGenBio, Seoul, Republic of Korea) containing a water-soluble tetrazolium salt, according to the manufacturer's instructions, on day 12.

2.6. Cell viability assessment

For 12 days, DMSO (0.01 %) or vitisin B (0.5 μM) were administered to senescent fibroblasts at 4-day intervals. As directed by the manufacturer, the Cedex HiRes analyzer (05650216001, Roche, Basel, Switzerland) was utilized (Huang et al., 2010).

2.7. Flow cytometric analysis of mitochondrial membrane potential (MMP), mitochondrial mass, lysosomal mass, autofluorescence, and autophagic flux

For 12 days, DMSO (0.01 %) or vitisin B (0.5 μM) were administered to senescent fibroblasts at 4-day intervals. In order to measure MMP, mitochondrial mass, and lysosomal mass, cells were treated for 30 min at 37°C with medium containing 0.6 μg/ml JC-10 (ENZ-52305, Enzo Life Sciences, Farmingdale, NY, USA), 50 nM MitoTracker™ Deep Red FM Dye (MTDR; M46753, Invitrogen, Waltham, MA, USA), and 500 nM LysoTracker™ Deep Red (LTDR) (L7526, Invitrogen). In order to measure autofluorescence, cells were exposed to dye-free medium for 30 min at 37°C. In order to measure autophagy flux, 20 μM chloroquine (CQ; C6628, Sigma, St. Louis, MO, USA) was added (w/) or not (w/o) 24 h prior to flow cytometry. The next step was to stain for 30 min using Cyto-ID staining solution (ENZ-51031–0050, Enzo Life Sciences). The mean fluorescence intensity is denoted by MFI. Autophagy flux is MFI Cyto-ID (w/ CQ) - MFI Cyto-ID (w/o CQ).

2.8. Western Blot Analysis

As previously mentioned, Western blot analysis was carried out (Park et al., 2025). Following antibodies were used (Table 1).

2.9. Analysis of oxygen consumption rate (OCR) and ATP production rate

Cells were seeded at a density of 5×10^4 cells per well in each well of an XF96 FluxPak (103793–100, Seahorse Bioscience, Billerica, MA, USA) and incubated for 16 h in a 37°C, 5 % CO_2 incubator. The medium

Table 2
Details of antibodies for immunofluorescence.

Antibody	Catalogue number	Dilution
LC3B antibody	A19665, Abclonal	1:200
OXPHOS cocktail antibody	ab110411, Abcam	1:200
Alexa Fluor® goat anti-mouse IgG antibody	A-28181, Invitrogen	1:200
Alexa Fluor® goat anti-rabbit IgG antibody	A-11008, Invitrogen	1:200

was then replaced with glucose-free XF Assay medium (102365–100, Seahorse Bioscience) and incubated for 1 h in the same incubator. Oxygen consumption rate (OCR) and ATP production rate were measured using a Seahorse Bioscience XFe96 flux analyzer with the Seahorse XF Cell Mito Stress Test Kit (101706–100, Seahorse Bioscience). Data were obtained from three independent experiments.

2.10. Immunofluorescence analysis

Senescent fibroblasts were treated with either DMSO (0.01 %) or vitisin B (0.5 μM) every 4 days for 12 days. Cells were permeabilized with 0.1 % Triton X-100 (X100RS, Sigma) for 15 min at room temperature (RT), followed by fixation with 4 % paraformaldehyde (252549, Sigma) for 15 min. Blocking was performed with PBS containing 10 % FBS for 1 h at RT. After adding the primary antibodies, the samples were incubated overnight at 4°C. After three washes with PBS, the samples were incubated with secondary antibodies for 1 h at RT. Photographs were taken using a Carl Zeiss LSM 700 confocal microscope (Carl Zeiss, Oberkochen, Germany). Following antibodies were used (Table 2).

2.11. Complementary DNA (cDNA) preparation and quantitative PCR (qPCR)

cDNA preparation and qPCR were carried out using the same methodology as our earlier investigation (Park et al., 2025). Table 1 summarizes the list of qPCR primers.

2.12. Measurement of β–defensin 2 expression

Immortalized human keratinocytes (HaCaT; 300493, Cytion, Eppelheim, Germany) were cultured in compliance with the procedures of previous studies (Yoon et al., 2024). To stimulate the expression of β-defensin 2, HaCaT cells were given 3 ng/ml interferon gamma (IFN-γ; PHC4031, Gibco, Waltham, MA, USA) and 6 ng/ml tumor necrosis factor-alpha (TNF-α; H8916, Sigma). To suppress the expression of β-defensin 2, HaCaT cells were given 15 ng/ml IL–4 (PHC0044, Gibco). HaCaT cells were then treated for 1 day to either DMSO (0.01 %) or vitisin B (0.5 μM).

2.13. Transcriptome expression profiling

For 12 days, senescent fibroblasts were treated with either DMSO (0.01 %) or vitisin B (0.5 μM) every 4 days. Paired-end expression of transcripts generated using TruSeq Small RNA on the Illumina platform was analyzed. Contaminants were removed to more accurately analyze the raw data obtained during the sequencing process. The cleaned data was mapped to the Homo sapiens (GRCh38, NCBI_109.20200522) genome using HISAT2 (version 2.1.0; Johns Hopkins University, Baltimore, MD, USA). Next, transcripts were assembled using StringTie (version 2.1.3b; Johns Hopkins University). Differentially expressed genes were identified through gene set enrichment analysis. A biological triplicate analysis was performed on each sample. The statistical threshold for determining statistical significance was a *p*-value of less than 0.05. Upon request, the raw RNA-sequencing data can be obtained from the corresponding author.

2.14. Lenti–virus production and infection

The pLK.O1 (#8453, Addgene, Watertown, MA, USA) vector backbone was used to generate shRNAs. Control shRNAs used the pLK.O1 backbone vector. shRNAs targeting WBP2NL were generated using the primer sets listed in Table 4. All shRNAs were produced using HiFi DNA Assembly Master Mix (E2621L, New Egland Biolab, Ipswich, MA, USA).

Table 3
Details of primers used in qPCR.

Target	Orientation	Sequence (5´-3´)	Size (bp)
36B4	forward	CAGCAAGTGGGAAGGTGTAATCC	23
(Accession number: NM_053275)	reverse	CCCATTCTATCATCAACGGGTACAA	25
IL–1β	forward	CCACAGACCTTCCAGGAGAATG	22
(Accession number: NM_000576.3)	reverse	GTGCAGTTCAGTGATCGTACAGG	23
IL–6	forward	CTGATGGGGTCAAATGAAGGTG	22
(Accession number: NM_000600.5)	reverse	CGTGCAACCATCCTCCAGAAC	21
IL–8	forward	CTGGCCGTGGCTCTCTTG	18
(Accession number: NM_000584.4)	reverse	CCTTGGCAAAACTGCACCTT	20
SAA1	forward	TCGTTCCTTGGCGAGGCTTTTG	22
(Accession number: NM_000331.6)	reverse	AGGTCCCCTTTTGGCAGCATCA	22
CCL5	forward	CCTGCTGCTTTGCCTACATTGC	22
(Accession number: NM_001278736.2)	reverse	ACACACTTGGCGGTTCTTTCGG	22
CXCL1	forward	AAACCGAAGTCATAGCCACACTC	23
(Accession number: NM_001511.4)	reverse	TCACTGTTCAGCATCTTTTCGATGATTT	28
p16	forward	CTCGTGCTGATGCTACTGAGGA	22
(Accession number: NM_000077)	reverse	GGTCGGCGCAGTTGGGCTCC	20
SLIT2	forward	CAGAGCTTCAGCAACATGACCC	22
(Accession number: NM_004787.4)	reverse	GAAAGCACCTTCAGGCACAACAG	23
Procollagen type I (Accession number: NM_002593.4)	forward	CAGACTGGCAACCTGAAGAAGTC	23
	reverse	TCGCCCCTGAGCTCGAT	17
COL1A1	forward	AGCAAGAACCCCAAGGACAA	20
(Accession number: NM_000088.4)	reverse	CGAACTGGAATCCATCGGTC	20
COL1A2	forward	CCTGGTGCTAAAGGAGAAAGAGG	23
(Accession number: NM_000089.4)	reverse	ATCACCACGACTTCCAGCAGGA	22
MMP-1	forward	ATGAAGCAGCCCAGATGTGGAG	22
(Accession number: NM_002421.4)	reverse	TGGTCCACATCTGCTCTTGGCA	22
β–defensin 2	forward	GTATCTCCTCTTCTCGTTCCTC	22
(Accession number: NM_004942.4)	reverse	GGATCGCCTATACCACCAAAAAC	23
WBP2NL	forward	ACAGAGCCTCACCTGCTGG	19
(Accession number: NM_152613.3)	reverse	TGAGAAGAGGAGGCAGAGGGAAG	23

Table 4
Details of primers used in shRNA plasmid engineering.

Target	Orientation	Sequence (5′–3′)	Size (bp)
Sh*WBP2NL*	forward	CCGGGGCAGGAAGAGAGATGAAATAATCAAGAGTTATTTCATCTCTCTTCCTGCTTTTTG	60
	reverse	AATTCAAAAAGCAGGAAGAGAGATGAAATAACTCTTGATTATTTCATCTCTCTTCCTGC	59

Table 5
The structure of phenylpropanoids used for screening.

Compound name	Structure	Molecular formular	Bioactivity
Calycosin–7–O–β–D–glucoside	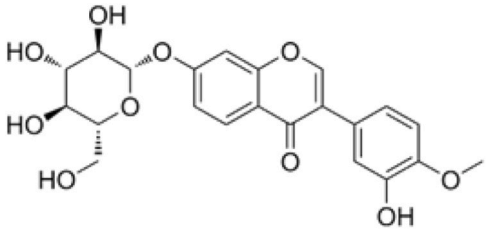	$C_{22}H_{22}O_{10}$	Antioxidants (Yan et al., 2019)
Oxypeucedanin	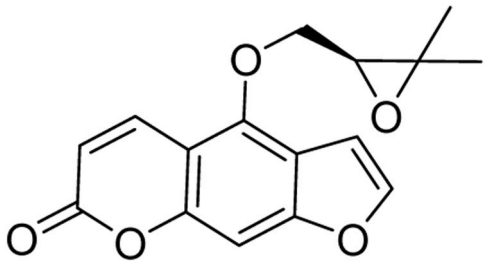	$C_{16}H_{14}O_5$	Antioxidants (Mottaghipisheh, 2021)
Vitisin B	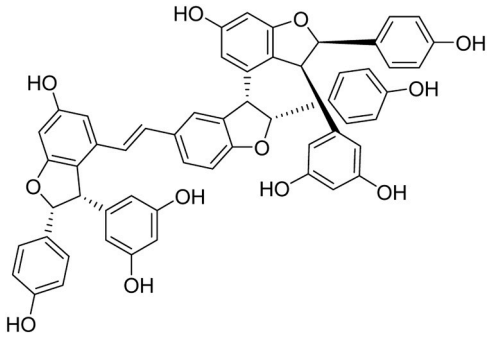	$C_{56}H_{42}O_{12}$	Antioxidants (Sy et al., 2023)

Lentiviruses expressing shRNAs were produced using human embryonic kidney 293 T cells (CRL-3216, ATCC) according to the procedure used in a previous study (Lee et al., 2024).

2.15. Statistics

For the statistical studies, GraphPad Prism 9 (San Diego, CA, USA) was utilized. The student's *t*-test and two–way ANOVA followed by Bonferroni's post–hoc test were used to determine whether the differences were significant.

3. Results

3.1. Vitisin B inhibits mitochondrial ROS generation in senescent fibroblasts

To identify natural compounds that can effectively reduce mitochondrial ROS generation, PPs (calycosin-7-O-β-D-glucoside, oxypeucedanin, and vitisin B) were used. Calycosin-7-O-β-D-glucoside is a flavonoid with antioxidant properties (Yan et al., 2019) (Table 5). Oxypeucedanin is a type of isoflavonoid possessing antioxidant activities (Mottaghipisheh, 2021) (Table 5). Vitisin B is a compound with a stilbene tetramer structure that has antioxidant properties (Sy et al., 2023) (Table 5). To determine the effect on mitochondrial ROS production, senescent fibroblasts were administered with the three PPs at 4 μM for 12 days. Then, mitochondrial hydroxyl radical levels were assessed using DHR123 (Henderson and Chappell, 1993). Resveratrol and young fibroblasts served as positive controls. As compared to DMSO-treated senescent fibroblast, resveratrol, a potent antioxidant, significantly decreased mitochondrial hydroxyl radicals (Fig. 1A). Young fibroblasts similarly demonstrated a significant decrease in mitochondrial hydroxyl radicals as compared to DMSO-treated senescent fibroblasts (Fig. 1A). Calycosine-7-O-β-D-glucoside, which has been known to have antioxidant activity, rather increased mitochondrial hydroxyl radicals (Fig. 1A). However, compared with the DMSO control, oxypeucedanin and vitisin B significantly decreased mitochondrial hydroxyl radicals (Fig. 1A). Among oxypeucedanin and vitisin B, vitisin B had a better antioxidant capacity in reducing mitochondrial hydroxyl radicals compared to resveratrol (Fig. 1A). These results suggest that vitisin B has the most prominent effect on reducing mitochondrial hydroxyl radicals among three PPs.

The discovery that vitisin B is effective in reducing mitochondrial ROS led to the investigation of the optimal concentration of vitisin B to reverse senescence. Since cell cycle arrest is a characteristic of

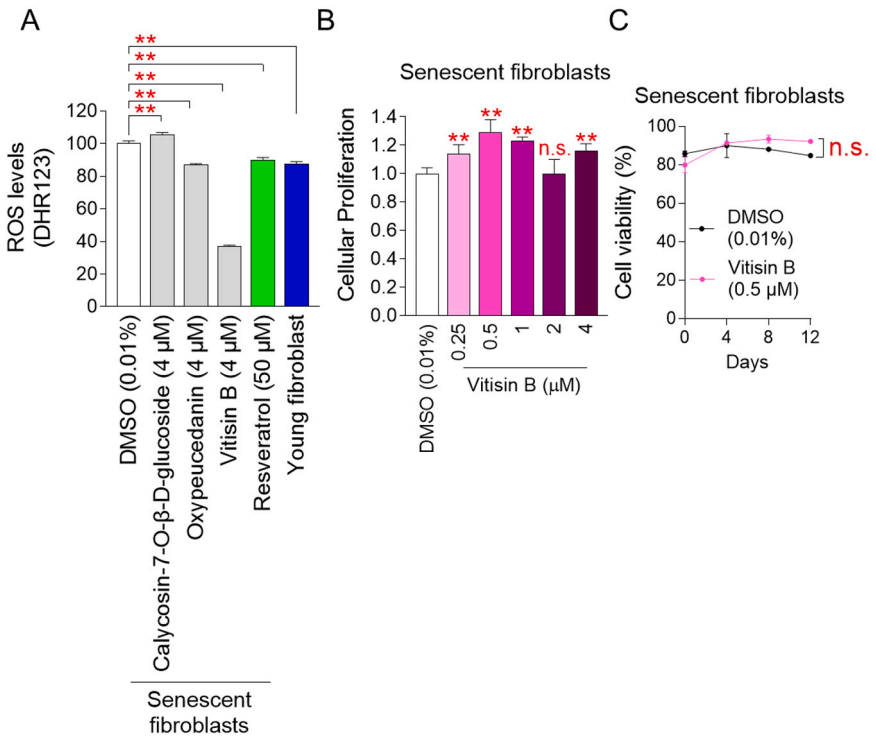

Fig. 1. Vitisin B inhibits mitochondrial ROS generation in senescent fibroblasts. (A) Mitochondrial hydroxyl radicals were measured in senescent fibroblasts treated with DMSO (0.01 %), calycosin-7-O-β-D-glucoside (4 μM), vitisin B (4 μM), or resveratrol (50 μM) for 12 days at 4-day intervals. Dihydrorhodamine 123 (DHR123) was used. Young fibroblasts served as positive controls. $^{**}P < 0.01$, Student's *t*–test. Mean ± S.D., $n = 3$. The representative flow graph of mitochondrial hydroxyl radicals was shown in Fig. S10. (B) Cellular proliferation was measured in senescent fibroblasts treated with DMSO (0.01 %) or vitisin B (0.5 μM) for 12 days at 4-day intervals. n.s. (not significant), $^{**}P < 0.01$, Student's *t*–test. Mean ± S.D., $n = 3$. (C) Cell viability was evaluated after 0, 4, 8, and 12 days of DMSO (0.01 %) or vitisin B (0.5 μM) treatment. n.s. (not significant), two–way ANOVA followed by Bonferroni's post–hoc test. Mean ± S.D., $n = 3$.

senescence (Poivre and Duez, 2017), we investigated the concentration at which vitisin B promotes proliferation. Vitisin B was given to senescent fibroblasts during 12 days at doses of 0.25, 0.5, 1, 2, and 4 μM. While 2 μM vitisin B did not increase proliferation compared to the DMSO control, 0.25, 0.5, 1, and 4 μM vitisin B significantly increased cell proliferation (Fig. 1B). Among the concentrations that significantly increased cell proliferation, 0.5 μM vitisin B promoted the greatest cell proliferation and was therefore selected as the optimal concentration for further studies.

Next, we measured cell viability to confirm the toxicity of vitisin B at the selected concentration (0.5 μM). The viability of senescent fibroblasts treated with 0.5 μM vitisin B and fibroblasts treated with DMSO was similar, indicating that vitisin B did not exhibit cytotoxicity (Fig. 1C).

3.2. *Vitisin B restores mitochondrial function*

The concentration utilized in the ROS-based screening (4 μM) was not the same as the concentration that was chosen (0.5 μM). Therefore, we examined whether the mitochondrial hydroxyl radicals-reducing effect was maintained at 0.5 μM vitisin B. Resveratrol and young fibroblasts served as positive controls. Resveratrol-treated senescent fibroblasts and young fibroblasts demonstrated a significant decrease in mitochondrial hydroxyl radicals compared to DMSO-treated senescent fibroblasts (Fig. 2A). Moreover, compared with the DMSO control, the 0.5 μM vitisin B significantly decreased mitochondrial hydroxyl radicals, suggesting that vitisin B has the ability to consistently reduce mitochondrial hydroxyl radicals even at 0.5 μM (Fig. 2A).

To determine whether vitisin B reduces other components of mitochondrial ROS besides mitochondrial hydroxyl radicals, MitoSOX, which detects mitochondrial superoxide anions, was used (Kauffman et al., 2016). Resveratrol-treated senescent fibroblasts and young fibroblasts demonstrated a significant decrease in mitochondrial superoxide anions compared to DMSO-treated senescent fibroblasts (Fig. 2B). Moreover, compared with the DMSO control, the 0.5 μM vitisin B significantly reduced mitochondrial superoxide anions, suggesting that vitisin B has the ability to reduce mitochondrial superoxide anions (Fig. 2B).

Since the most prominent mitochondrial damage induced by ROS is the reduction in mitochondrial membrane potential (MMP) (Sherratt, 1991), we investigated the effect of vitisin B on MMP. Compared with DMSO-treated senescent fibroblasts, resveratrol did not significantly reduce MMP (Fig. 2C). However, young fibroblasts demonstrated a significant increase in MMP as compared to DMSO-treated senescent fibroblasts (Fig. 2C). Moreover, compared with the DMSO control, vitisin B significantly increased MMP, indicating the mitochondrial functional recovery by vitisin B (Fig. 2C).

MMP is a proton motive force that enable oxidative phosphorylation (OXPHOS) (Mitchell and Moyle, 1967). Since we found that MMP was increased by vitisin B, we evaluated the OXPHOS efficiency through OCR measurement (Plitzko and Loesgen, 2018). Sequential injections of oligomycin, carbonyl cyanide-p-trifluoromethoxyphenylhydrazone (FCCP), and rotenone/antimycin A were applied to evaluate non-mitochondrial respiration, maximal respiration, and ATP-coupled respiration, respectively (Mookerjee et al., 2017). Young fibroblasts served as positive controls. The observed OCR values of young fibroblasts were lower than those of DMSO-treated senescent fibroblasts, indicating that young fibroblasts consume less oxygen through efficient OXPHOS (Fig. 2D). However, the observed OCR values were restored to those of young fibroblasts upon vitisin B treatment, indicating the vitisin B-mediated efficient OXPHOS (Fig. 2D).

Young fibroblasts increase ATP production via OXPHOS and decrease it via glycolysis, whereas senescent fibroblasts decrease it via OXPHOS and increase it via glycolysis (Lee et al., 2021). Since we found

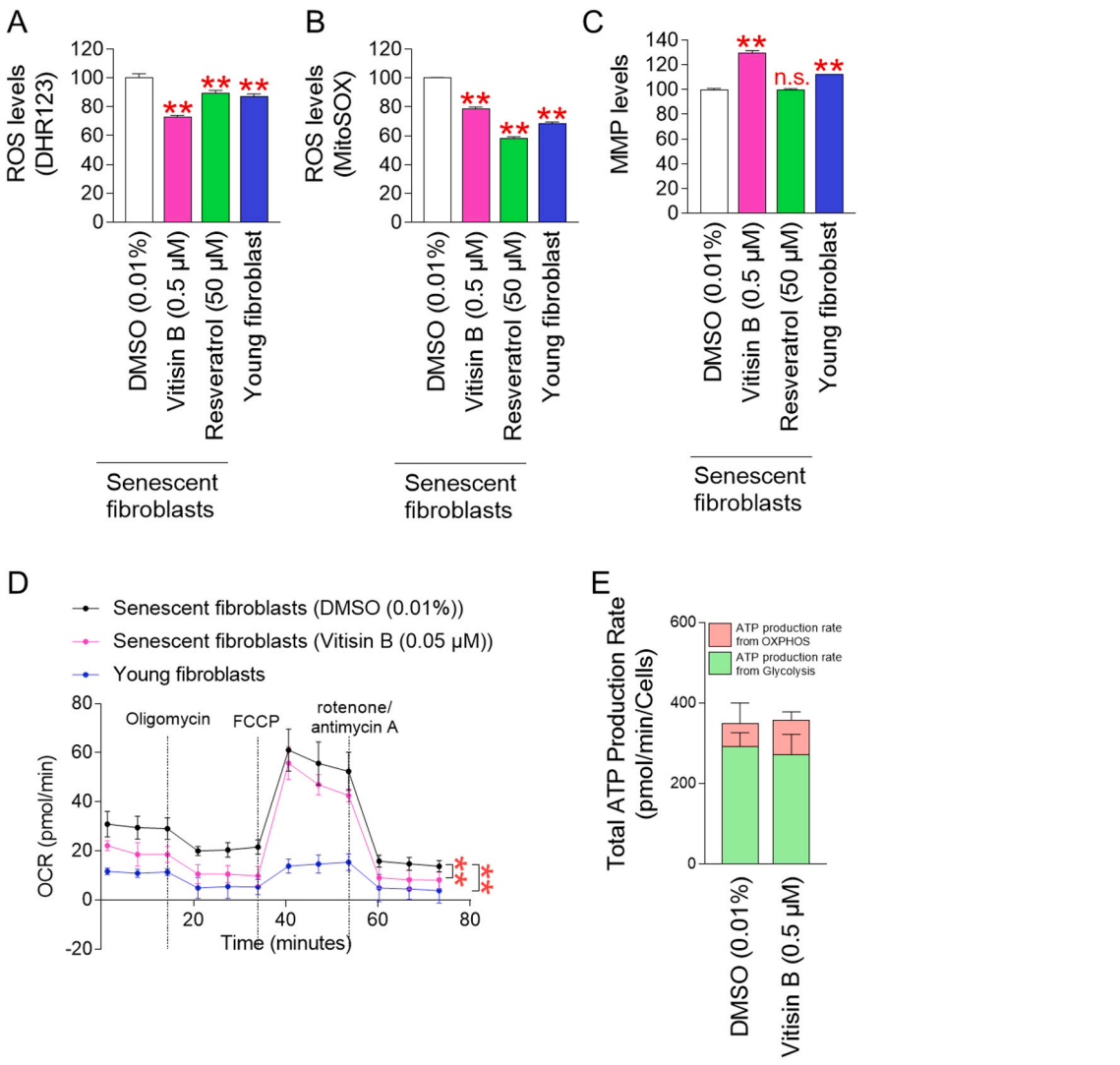

Fig. 2. Vitisin B restores mitochondrial function. (A and B) Mitochondrial hydroxyl radicals and mitochondrial superoxide anions were measured in senescent fibroblasts treated with DMSO (0.01 %), vitisin B (0.5 μM) or resveratrol (50 μM) for 12 days at 4-day intervals. DHR123 and MitoSOX was used. Young fibroblasts served as positive controls. $^{**}P < 0.01$, Student's *t*–test. Mean ± S.D., $n = 3$. Representative flow graphs of mitochondrial hydroxyl radicals and mitochondrial superoxide anions were shown in Fig. S11 and Fig. S12, respectively. (C) MMP levels were measured in senescent fibroblasts treated with DMSO (0.01 %), vitisin B (0.5 μM) or resveratrol (50 μM) for 12 days at 4-day intervals. Young fibroblasts served as positive controls. $^{**}P < 0.01$, Student's *t*–test. Mean ± S.D., $n = 3$. The representative flow graph of MMP levels was shown in Figure S13. (D) Oxygen consumption rate (OCR; pmol/min) was assessed in senescent fibroblasts treated with DMSO (0.01 %) or vitisin B (0.5 μM) for 12 days at 4-day intervals. Young fibroblasts served as positive controls. ** $p < 0.01$, two–way ANOVA followed by Bonferroni's post hoc test. Means ± S.D., $n = 3$. (E) Total ATP production rate was measured in senescent fibroblasts treated with DMSO (0.01 %) or vitisin B (0.5 μM) for 12 days at 4-day intervals. The rate at which OXPHOS produces ATP is indicated by the pink square. The rate at which glycolysis produces ATP is indicated by the green square. Mean ± S.D., $n = 3$.

that the OXPHOS efficiency was increased by vitisin B, we evaluated the ATP production rate, an indicator of mitochondrial function. Vitisin B increased ATP production via OXPHOS and decreased it via glycolysis, indicating that vitisin B restores mitochondrial function (Fig. 2E).

3.3. *Vitisin B eliminates dysfunctional mitochondria through mitophagy*

The discovery that vitisin B restores mitochondrial function raised questions about how vitisin B achieves this restoration. Damaged mitochondria are eliminated by mitophagy, which restores mitochondrial function (Picca et al., 2023). Thus, we hypothesized that vitisin B activates mitophagy to remove dysfunctional mitochondria, thereby restoring mitochondrial function. Since mitophagy selectively eliminates dysfunctional mitochondria using autophagosomes (Picca et al., 2023), we analyzed mitophagy by observing the co-localization of mitochondria with microtubule-associated protein 1 A/1B-light chain 3B (LC3B), a membrane protein of autophagosomes (Chen et al., 2010). Young fibroblasts showed a significantly increased colocalization expression of LC3B and mitochondria compared to DMSO-treated senescent fibroblasts (Figure S14; white arrows). Colocalization significantly reappeared after treatment with vitisin B in senescent fibroblasts (Figure S14; white arrows). To further confirm the role of vitisin B in mitophagy, cells were treated with chloroquine (CQ) 24 h before immunofluorescence analysis. CQ alters the pH of lysosomes, inducing the accumulation of autophagosomes (Mauthe et al., 2018). As expected, the CQ-treated group (Fig. 3A; white arrows) showed increased accumulation of autophagosomes (LC3B, green) compared to the untreated group (Figure S14; white arrows). Moreover, senescent fibroblasts co-treated with CQ and vitisin B significantly increased colocalization compared to senescent fibroblasts co-treated with CQ and DMSO (Fig. 3A; white arrows). These data indicate that vitisin B promotes mitophagy activation.

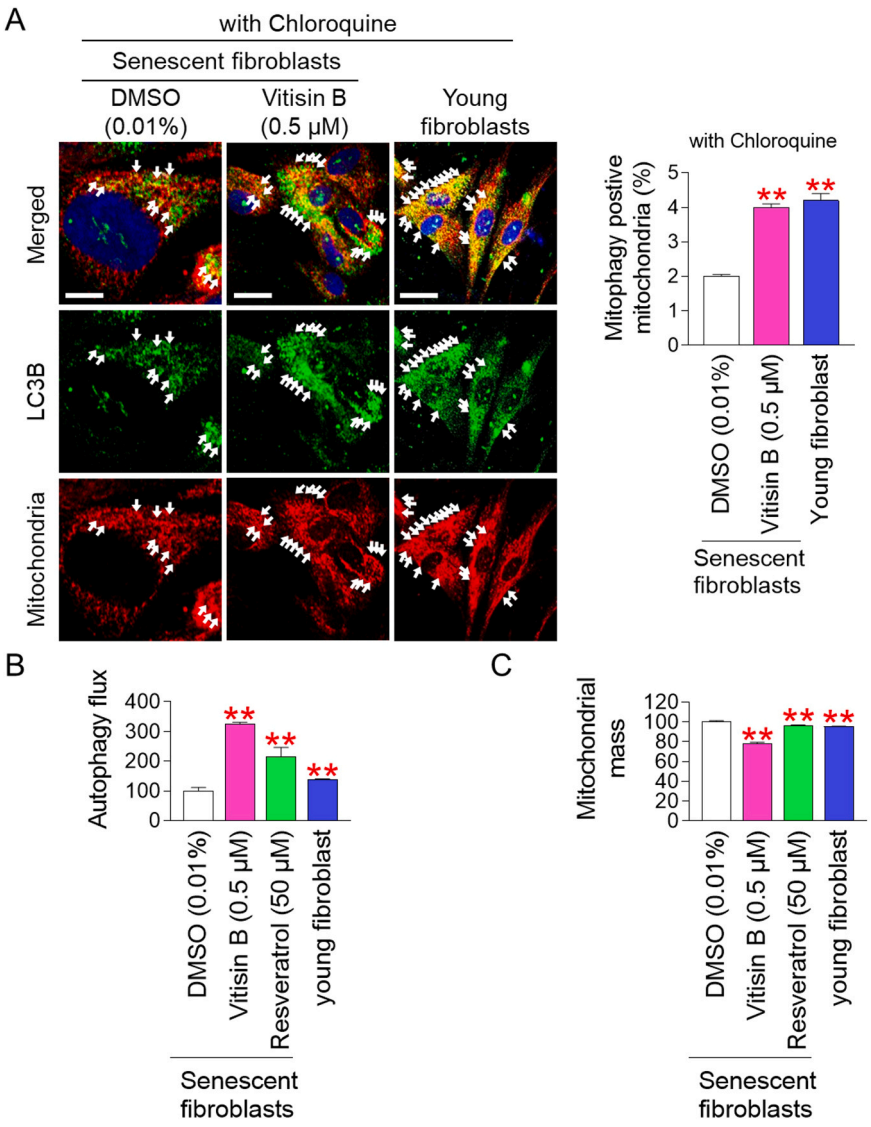

Fig. 3. Vitisin B eliminates dysfunctional mitochondria through mitophagy. (A) Immunostaining for LC3B (green) and mitochondria (red) was conducted in senescent fibroblasts treated with DMSO (0.01 %) or vitisin B (0.5 μM) for 12 days at 4-day intervals. Young fibroblasts served as positive controls. 20 μM chloroquine was added to cells 24 h before immunofluorescence analysis. Scale bar 10 μm. Mitophagy is indicated by a white arrow. $^{**}P < 0.01$, Student's *t*–test. Mean ± S.D., $n = 3$. (B and C) Autophagy flux and mitochondrial mass were measured in senescent fibroblasts treated with DMSO (0.01 %) or vitisin B (0.5 μM) for 12 days at 4-day intervals. $^{**}P < 0.01$, Student's *t*–test. Mean ± S.D., $n = 3$. Representative flow graphs of autophagy flux and mitochondrial mass were shown in Fig. S15 and Fig. S16, respectively.

We then measured autophagy flux to quantitatively measure mitophagy activation. Autophagy flux is one way to measure mitophagy activation, as it indicates the rate at which autophagy, including mitophagy, removes damaged organelles (Zhang, 2013). Resveratrol and young fibroblasts served as positive controls. Resveratrol-treated senescent fibroblasts and young fibroblasts demonstrated a significant increase in autophagy flux compared to DMSO-treated senescent fibroblasts (Fig. 3B). Moreover, compared with the DMSO control, vitisin B significantly increased autophagy flux (Fig. 3B).

Autophagy flux refers to the rate at which damaged organelles are eliminated. Thus, to evaluate whether mitophagy eliminates mitochondria, mitochondrial mass was measured. Resveratrol-treated senescent fibroblasts and young fibroblasts demonstrated a significant decrease in mitochondrial mass compared to DMSO-treated senescent fibroblasts (Fig. 3C). Moreover, compared with the DMSO control, vitisin B significantly decreased mitochondrial mass, indicating activated mitophagy (Fig. 3C).

An increase in the LC3-II protein is a common marker for autophagy, as it indicates an increase in the number of autophagosomes (Mizushima and Yoshimori, 2007). To confirm vitisin B-mediated activation of mitophagy, a Western blot for LC3-II was performed. Compared with the DMSO control, vitisin B markedly increased the expression of LC3-II, supporting vitisin B-mediated activation of mitophagy (Figure S17).

3.4. *Vitisin B ameliorates senescence-associated phenotypes*

One of the requirements for senescence rejuvenation is the restoration of mitochondrial function (Kim et al., 2019; Kuk et al., 2023; Lee et al., 2022, 2021; Park et al., 2022). The finding that vitisin B restores mitochondrial function led to the evaluation of the effects of vitisin B on senescence. Lipofuscin, a cross-linked protein residue generated by iron-catalyzed oxidation, is resistant to destruction and accumulates in lysosomes during senescence (Ilie et al., 2020). Therefore, we investigated the effect of vitinicin B on lipofuscin (Ilie et al., 2020). Lipofuscin was examined by measuring autofluorescence (Davan-Wetton and Montero-Melendez, 2024). Young fibroblasts served as positive controls.

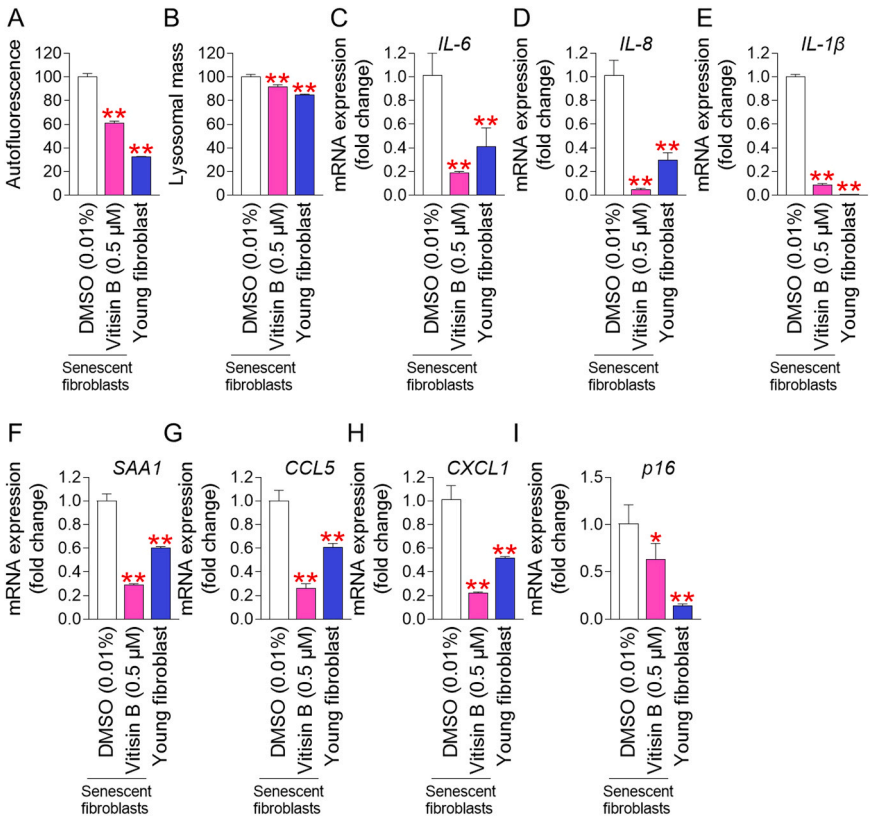

Fig. 4. Vitisin B ameliorates senescence-associated phenotypes. (A and B) Autofluorescence and lysosomal mass were measured in senescent fibroblasts treated with DMSO (0.01 %) or vitisin B (0.5 μM) for 12 days at 4-day intervals. Young fibroblasts served as positive controls. $^{**}P < 0.01$, Student's *t*–test. Mean ± S.D., $n = 3$. Representative flow graphs of autofluorescence and lysosomal mass were shown in Fig. S18 and Fig. S19, respectively. (C–F) mRNA expression levels of *IL-6*, *IL-8*, *IL-1β*, *SAA1*, *CCL5*, *CXCL1*, and *p16* were measured in senescent fibroblasts treated with DMSO (0.01 %) or vitisin B (0.5 μM) for 12 days at 4-day intervals. Young fibroblasts served as positive controls. $^{**}P < 0.01$, Student's *t*–test. Mean ± S.D., $n = 3$.

Young fibroblasts showed a significant reduction in autofluorescence compared to DMSO-treated senescent fibroblasts control (Fig. 4A). Moreover, compared with the DMSO control, vitisin B significantly reduced autofluorescence, indicating that vitisin B effectively reduces lipofuscin accumulation (Fig. 4A).

Lipofuscin-filled lysosomes reduce lysosomal activity by serving as a "sink" for newly generated lysosomal enzymes (Brunk and Terman, 2002). To compensate for the reduced lysosomal activity, lysosomal mass increases (Brunk and Terman, 2002). To determine whether vitisin B affects lysosomal activity, we analyzed the effect of vitisin B on lysosomal mass. Young fibroblasts showed a significant decrease in lysosomal mass compared to DMSO-treated senescent fibroblasts (Fig. 4B). Moreover, compared with the DMSO control, vitisin B significantly decreased lysosomal mass, indicating that vitisin B increases lysosomal activity (Fig. 4B).

In the mitochondrial cytosol, ROS interacts with mitochondrial superoxide dismutase to convert superoxide into hydrogen peroxide, which can penetrate the outer membrane of the mitochondria and harm proteins in the cytosol (Dan Dunn et al., 2015). This reaction triggers the release of senescence-associated secretory phenotype (SASP) (Ichimura et al., 2003; Naik and Dixit, 2011; Nelson et al., 2018). To determine whether vitisin B affects SASP, we analyzed the effect of vitisin B on the expression of inflammatory cytokines, *IL-6*, *IL-8*, and *IL-1β*. Young fibroblasts demonstrated a significant decrease in the expression of *IL-6*, *IL-8*, and *IL-1β* compared to DMSO-treated senescent fibroblasts (Fig. 4C, D, and E). Moreover, compared with the DMSO control, vitisin B significantly decreased the expression of *IL-6*, *IL-8*, and *IL-1β* (Fig. 4C, D, and E).

Serum amyloid A1 (SAA1) is one of the SASP components and is involved in the progression of senescence (Ebert et al., 2015). Young fibroblasts demonstrated a significant decrease in *SAA1* expression compared to DMSO-treated senescent fibroblasts (Fig. 4F). Moreover, compared with the DMSO control, vitisin B significantly reduced *SAA1* expression (Fig. 4F).

C–C motif chemokine ligand 5 (*CCL5*) is a key component of SASP and is released by senescent cells to promote inflammation (Wang et al., 2023). *C-X-C motif chemokine ligand 1* (*CXCL1*) is a prominent chemokine component of SASP (Ullah et al., 2024). Young fibroblasts demonstrated a significant decrease in the expression of *CCL5* and *CXCL1* compared to DMSO-treated senescent fibroblasts (Fig. 4G and H). Moreover, compared with the DMSO control, vitisin B significantly reduced the expression of *CCL5* and *CXCL1* (Fig. 4G and H).

p16 is a key pathway regulating cell cycle arrest (González-Gualda et al., 2021). p16 also plays a crucial role in maintaining the senescent state (Huang et al., 2022). As previously observed (Kang et al., 2017), young fibroblasts demonstrated a significant decrease in *p16* expression compared to DMSO-treated senescent fibroblasts (Fig. 4I). Moreover, compared with the DMSO control, vitisin B significantly reduced *p16* expression, indicating the vitisin B-mediated cell cycle progression (Fig. 4I).

ROS harm proteins important in DNA maintenance or directly damage DNA (Checa and Aran, 2020). Our finding that vitisin B reduces mitochondrial ROS production prompted us to investigate the effects of vitisin B on DNA damage. Since decreased expression of phospho-Ataxia-telangiectasia mutated (p-ATM) is indicative of reduced DNA damage (Gilbreath et al., 2021), expression of p-ATM was examined. Compared with the DMSO control, vitisin B markedly decreased the expression of p-ATM in senescent fibroblasts, suggestive of decreased DNA damage (Figure S20).

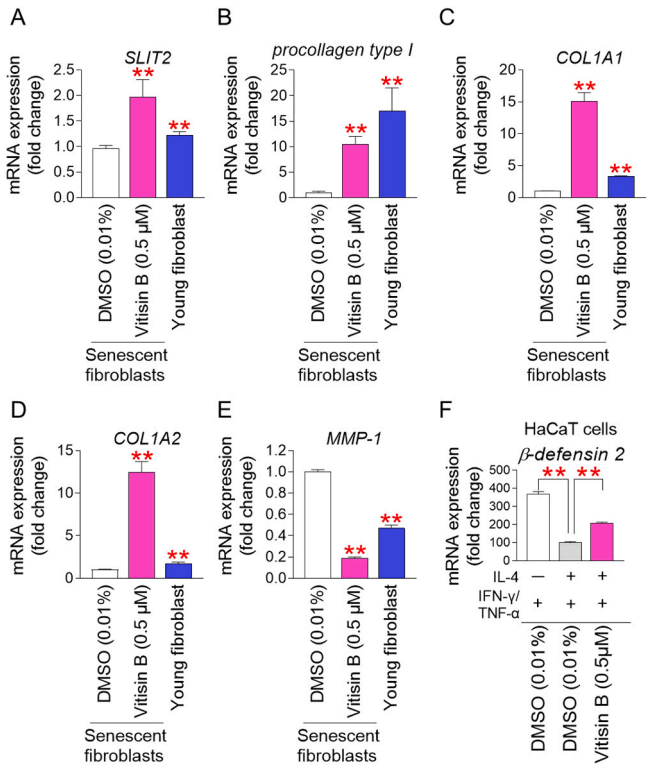

Fig. 5. Vitisin B restores the expression of genes involved in skin regeneration to the level of young fibroblasts. (A–E) mRNA expression levels of *SLIT2*, *procollagen type I*, *COL1A1*, *COL1A2*, and *MMP-1* were measured in senescent fibroblasts treated with DMSO (0.01 %) or vitisin B (0.5 μM) for 12 days at 4-day intervals. Young fibroblasts served as positive controls. $^{**}P < 0.01$, Student's *t*–test. Mean ± S.D., $n = 3$. (F) IFN-γ (10 ng/ml) and TNF-α (20 ng/ml) were administered to HaCaT cells. After then, 50 ng/ml IL-4 was administered to HaCaT cells. For 1 day, HaCaT cells were administered to either DMSO (0.01 %) or vitisin B (0.5 μM). Measurement of expression of *β-defensin 2*. $^{**}P < 0.01$, Student's *t*–test. Mean ± S.D., $n = 3$.

3.5. *Vitisin B restores the expression of genes involved in skin regeneration to the level of young fibroblasts*

The discovery that vitisin B improves senescence-associated phenotypes led to an evaluation of the effects of vitisin B on genes involved in skin regeneration. Slit-inducing ligand 2 (SLIT2) controls cell-cell interactions to promote the regeneration of skin tissue (Kim et al., 2023b; Wu et al., 2017). When SLIT2 expression is downregulated, the epidermal barrier's ability to regenerate tissue is compromised (Kim et al., 2023b; Wu et al., 2017). Young fibroblasts demonstrated a significant increase in *SLIT2* expression as compared to DMSO-treated senescent fibroblasts (Fig. 5A). Moreover, compared with the DMSO control, vitisin B significantly increased *SLIT2* expression, suggesting that vitisin B activates genes involved in skin regeneration (Fig. 5A).

A reduction in collagen synthesis, which results in a reduction in the structural support of the skin barrier, is one of the main markers of skin aging (Quan and Fisher, 2015). To evaluate the effect of vitisin B on collagen synthesis, the expression levels of *procollagen type I*, *type I collagen alpha 1* (*COL1A1*), and *type I collagen alpha 2* (*COL1A2*) were examined. Young fibroblasts demonstrated a significant increase in the expression of *pro-COL1*, *COL1A1*, and *COL1A2* as compared to DMSO-treated senescent fibroblasts (Fig. 5B, C, and D). Moreover, compared with the DMSO control, vitisin B significantly increased the expression of *pro-COL1*, *COL1A1*, and *COL1A2*, indicating that vitisin B improves the structural support of the skin (Fig. 5B, C, and D).

Skin barrier function is impaired by increased expression of matrix metalloproteinase 1 (MMP-1), which enhances collagen degradation (Pittayapruek et al., 2016). The discovery that vitisin B stimulates collagen synthesis prompted us to evaluate the effect of vitisin B on *MMP-1* expression. Young fibroblasts demonstrated a significant decrease in the expression of *MMP-1* as compared to DMSO-treated senescent fibroblasts (Fig. 5E). Moreover, compared with the DMSO control, vitisin B significantly decreased *MMP-1* expression, suggesting that vitisin B inhibits collagen degradation (Fig. 5E).

Lesional skin protects itself by increasing the expression of an antimicrobial peptide called β-defensin 2 (Semple and Dorin, 2012). IFN-γ/TNF-α-mediated inflammatory signaling induces β-defensin 2 expression in keratinocytes, but IL-4 inhibits this induction (Piipponen et al., 2020). Therefore, keratinocytes (HaCaT cells) were administered with IFN-γ/TNF-α to induce β-defensin 2 expressions. Then, HaCaT cells were administered with IL-4. IFN-γ/TNF-α-induced *β-defensin 2* expression was reduced by IL-4 administration (Fig. 5F). However, administration of vitisin B significantly increased the expression of *β-defensin 2*, suggesting that vitisin B enhances the antibacterial activity of the skin (Fig. 5F).

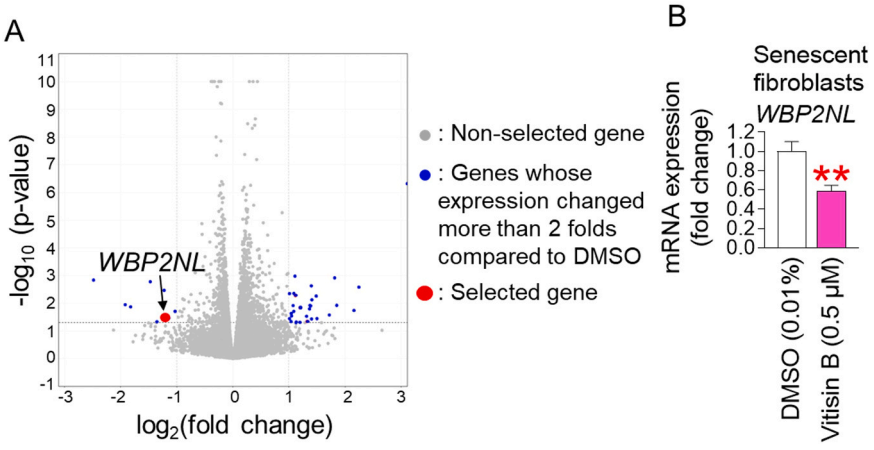

Fig. 6. *WBP2NL* functions as a critical regulator of the vitisin B-mediated senescence amelioration. (A) Compared with the DMSO control group, DEG analysis showed that 39 genes were significantly changed by more than 2-fold (blue dots). Among the 39 genes, *WBP2NL* was selected as a key candidate because it showed the greatest decrease (red dots). Unselected genes: gray dots. (B) *WBP2NL* expression levels were measured in senescent fibroblasts treated with DMSO (0.01 %) or vitisin B (0.5 μM) for 12 days at 4-day intervals. $^{**}P < 0.01$, Student's *t*–test. Mean ± S.D., $n = 3$.

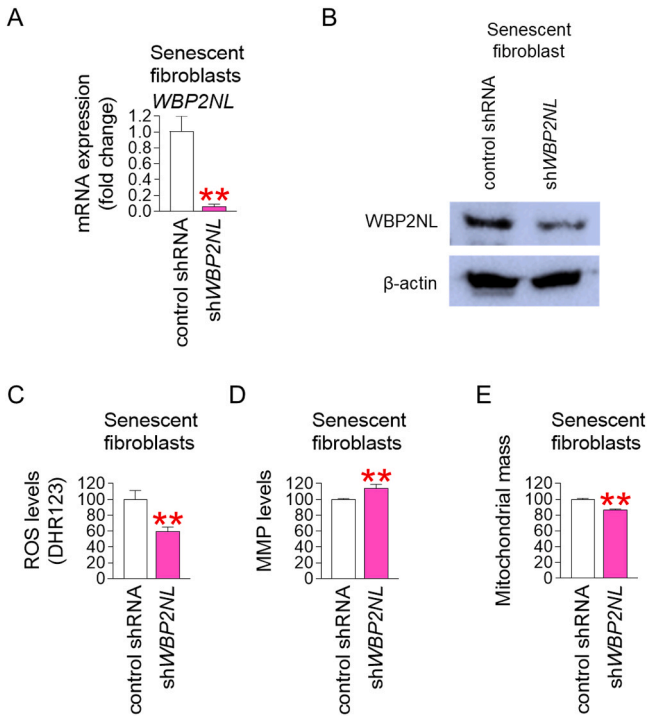

Fig. 7. *WBP2NL* knockdown restores mitochondrial function. (A) mRNA expression levels of *WBP2NL* were measured in senescent fibroblasts transduced with lentivirus expressing control shRNA or *WBP2NL* shRNA. $^{**}P < 0.01$, Student's *t*–test. Means ± S.D., $n = 3$. (B) Expression levels of WBP2NL protein were measured in senescent fibroblasts transduced with lentivirus expressing control shRNA or *WBP2NL* shRNA. (C) Mitochondrial hydroxyl radicals were measured in senescent fibroblasts transduced with lentivirus expressing control shRNA or *WBP2NL* shRNA. $^{**}P < 0.01$, Student's *t*–test. Means ± S.D., $n = 3$. The representative flow graph of mitochondrial hydroxyl radicals was shown in Fig. S22. (D) MMP was measured in senescent fibroblasts transduced with lentivirus expressing control shRNA or *WBP2NL* shRNA. $^{**}P < 0.01$, Student's *t*–test. Means ± S.D., $n = 3$. The representative flow graph of MMP was shown in Fig. S23. (E) Mitochondrial mass was measured in senescent fibroblasts transduced with lentivirus expressing control shRNA or *WBP2NL* shRNA. $^{**}P < 0.01$, Student's *t*–test. Means ± S.D., $n = 3$. The representative flow graph of mitochondrial mass was shown in Figure S24.

3.6. *WBP2NL functions as a critical regulator of the vitisin B-mediated senescence amelioration*

The discovery that vitisin B induces senescence recovery led to the elucidation of the senescence reversal mechanism by vitisin B. We performed RNA sequencing and then used transcriptome sequencing data to select differentially expressed genes (DEG). The DEG analysis identified that 39 genes were significantly changed by more than 2-fold (blue dots, Table S1 and Fig. 6A). Among the 39 genes, WBP2 N-terminal homologous protein (WBP2NL; Accession Number: NM_152613.3), which showed the greatest decrease (red dots, 5.6-fold decrease compared to the DMSO control group, Table S1 and Fig. 6A), was selected as a candidate gene. WBP2NL, the peri–acrosomal WW–domain binding protein, is an essential component in the regulation of signal transduction (Buffa et al., 2013). *WBP2NL* expression was significantly lower in the vitisin B-treated group than in the DMSO control (Fig. 6B). Therefore, *WBP2NL* was selected as a candidate gene in vitisin B-mediated senescence amelioration,

3.7. *WBP2NL knockdown restores mitochondrial function*

The finding that *WBP2NL* is a candidate for the anti-senescence effect of vitisin B prompted us to examine whether *WBP2NL* knockdown could produce similar effects. To this end, we established a lentiviral system expressing shRNA targeting *WBP2NL* or control shRNA. Then, senescent fibroblasts were infected with the lentiviral system to confirm whether shRNA targeting *WBP2NL* suppressed *WBP2NL* expression. Compared with the control shRNA group, shRNA targeting *WBP2NL* group demonstrated a significant decrease in *WBP2NL* expression, suggesting that efficient *WBP2NL* knockdown by shRNA was achieved (Fig. 7A).

The discovery of suppression of *WBP2NL* expression by shRNA targeting *WBP2NL* prompted us to evaluate the effect of shRNA on WBP2NL protein expression. Compared to the control shRNA group, the *WBP2NL*-targeting shRNA group markedly suppressed WBP2NL protein expression (Fig. 7B).

We then evaluated the impact of *WBP2NL* knockdown on mitochondrial hydroxyl radicals. Compared to the control shRNA group, the shRNA targeting *WBP2NL* group significantly decreased mitochondrial hydroxyl radicals (Fig. 7C). These results suggest that *WBP2NL* knockdown exhibits a mitochondrial ROS-reducing effect similar to vitisin B.

Since the reduction of mitochondrial ROS indicates the recovery of mitochondrial function, we examined MMP, which is the factor that indicates mitochondrial function. The shRNA targeting *WBP2NL* group significantly increased MMP compared to the control shRNA group (Fig. 7D).

As a feedback mechanism, ROS-induced mitochondrial dysfunction causes an increase in mitochondrial mass (Lee et al., 2002; Passos et al., 2007). Thus, we examined the effect of *WBP2NL* knockdown on mitochondrial mass. Compared to the control shRNA group, the shRNA targeting *WBP2NL* group significantly reduced mitochondrial mass (Fig. 7E). These results suggest that *WBP2NL* knockdown reduced mitochondrial mass similar to vitisin B.

Because p62 (also known as SQSTM1) is selectively degraded by autophagy, its reduction reflects increased autophagic activity, making it a reliable marker for monitoring autophagic flux (Bjørkøy et al., 2009). Thus, we evaluated the effect of *WBP2NL* knockdown on autophagic activity by examining the p62 expression. Compared to the control shRNA group, the shRNA targeting *WBP2NL* group markedly decreased p62 protein expression, indicating *WBP2NL* knockdown activates autophagic activity (Figure S21).

3.8. *WBP2NL knockdown restores senescence-associated phenotypes*

To investigate the effect of *WBP2NL* knockdown on SASP, the expression of SASP-related genes was analyzed. Compared to the control shRNA group, the shRNA targeting *WBP2NL* group significantly decreased the expression of *IL-6*, *IL-8*, and *IL-1β* (Fig. 7A–C). In addition, compared to the control shRNA group, the shRNA targeting *WBP2NL* group significantly decreased the expression of *SAA1* (Fig. 7D).

To investigate the effect of *WBP2NL* knockdown on cell cycle progression, the expression of *p16* was evaluated. Compared to the control shRNA group, the shRNA targeting *WBP2NL* group significantly decreased the expression of *p16* expression (Fig. 7E).

To investigate the effect of *WBP2NL* knockdown on genes involved in skin regeneration, the expression of *procollagen type I* and *MMP-1* was evaluated. Compared to the control shRNA group, the shRNA targeting *WBP2NL* group significantly increased the expression of *procollagen type I* and decreased the expression of *MMP-1* (Fig. 7E and F).

4. Discussion

The organelle that produces approximately 90 % of ROS is the mitochondria (Tirichen et al., 2021). Complexes in ETC are the main sites of ROS generation. Specifically, complex I converts oxygen molecules to superoxide anion, which is discharged into the mitochondrial matrix. Complex III converts oxygen molecules to superoxide anion, which is discharged into the mitochondrial matrix and intermembrane space (Turrens, 2003). Mitochondrial dysfunction reduces the activity of ETC complexes, impeding electron transport and increasing electron

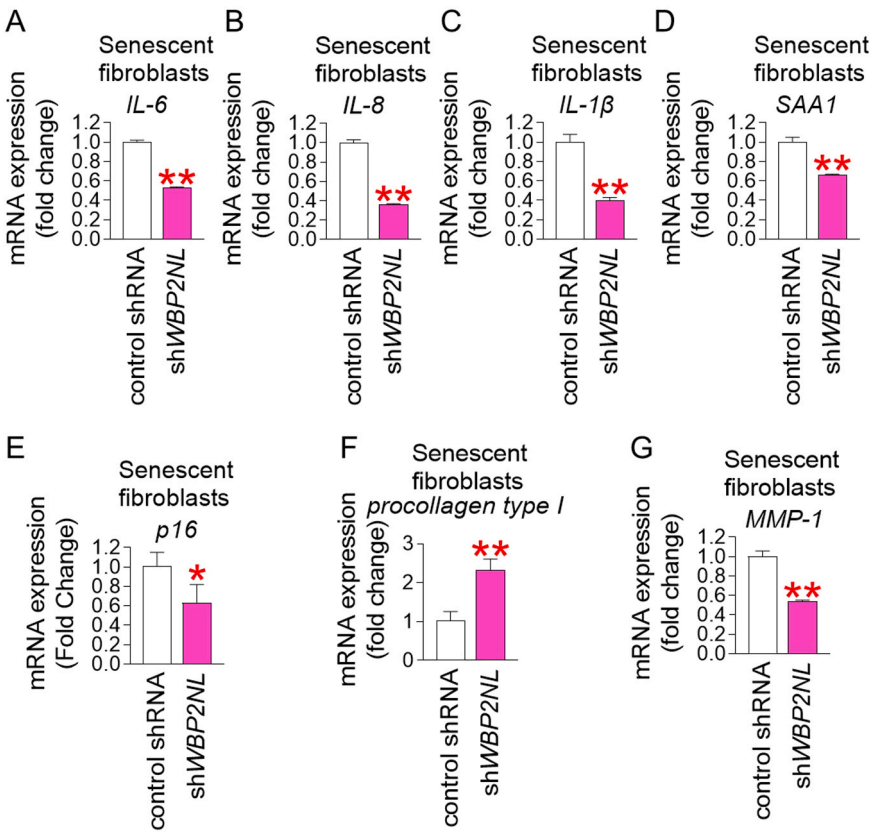

Fig. 8. *WBP2NL* knockdown restores senescence-associated phenotypes. (A–E) Expression levels of *IL-6*, *IL-8*, *IL-1β*, *SAA1*, and *p16* were measured in senescent fibroblasts transduced with lentivirus expressing control shRNA or *WBP2NL* shRNA. $^{**}P < 0.01$, Student's *t*–test. Means ± S.D., $n = 3$. (F and G) Expression levels of *procollagen type I* and *MMP-1* were measured in senescent fibroblasts transduced with lentivirus expressing control shRNA or *WBP2NL* shRNA. $^{**}P < 0.01$, Student's *t*–test. Means ± S.D., $n = 3$.

leak to oxygen, thereby increasing superoxide anion production (Nakai and Tsuruta, 2021). The increased ROS production further impairs ETC function, starting a vicious cycle that increases superoxide anion production (Lee et al., 2023). This vicious cycle causes organelle dysfunction, ultimately resulting in senescence (Stout and Birch-Machin, 2019). This causal link implies that lowering mitochondrial ROS generation is a crucial tactic to restore senescence (Lee et al., 2023). Here, we found that vitisin B reduces ROS generation in mitochondria. Specifically, the increase in MMP induced by vitisin B led to an increase in ATP production through OXPHOS, which indicates efficient electron transfer in the ETC (Nolfi-Donegan et al., 2020). The effective electron transfer lowers electron leakage, thereby reducing the generation of mitochondrial ROS (Zhao et al., 2019). Here, we identified a novel mechanism by which vitisin B reduces ROS production in mitochondria. These findings will provide evidence for the possibility of treating aging by reducing mitochondrial ROS production.

PPs are secondary metabolites derived from the shikimate pathway using phenylalanine and tyrosine (Korkina, 2007). PPs can be classified into five groups: coumarins, flavonoids, phenols, stilbenes, and lignins (De Rossi et al., 2025). Calycosin-7-O-β-D-glucoside, oxypeucedanin, and vitisin B used in this experiment also belong to PPs. Calycosin-7-O-β-D-glucoside has a hydroxyl group in the isoflavone skeleton, which is a type of flavonoid (Yan et al., 2019). Oxypeucedanin is a coumarin skeleton with a methoxy group, a hydroxyl group, and a methyl group (Mottaghipisheh, 2021). Vitisin B, which has a stilbene tetramer structure, has four hydroxyl groups that contribute to its radical scavenging property (Sy et al., 2023). Among the three PPs, vitisin B showed the most significant inhibition of mitochondrial ROS production. This may be due to the structural features of vitisin B. For example, calicosin-7-O-β-D-glucoside has a glucose moiety attached to the phenol group, which may hinder the direct interaction with ROS and weaken its ability to scavenge reactive oxygen species (Xiao, 2017). Oxypeucedanin contains a coumarin ring, which may limit electron delocalization and thus limit its reactivity with reactive oxygen species (ROS) (Nguyen and Grabow, 2020). However, vitisin B, which has a stilbene tetramer structure, has four hydroxyl groups that can effectively neutralize free radicals by donating electrons (Sy et al., 2023). The structural characteristics of vitisin B maximizes the antioxidant efficacy by exposing vitisin B to more ROS binding. In summary, the antioxidant efficacy of PPs varies depending on the number of hydroxyl groups and the type of functional groups contributing to the radical scavenging ability. Therefore, it is expected that additional modifications of the number of hydroxyl groups contributing to the radical scavenging ability of vitisin B will further increase the antioxidant efficacy. However, we admit that additional research is required to validate this hypothesis.

ROS-mediated oxidative stress is a major inducer of age-related inflammation, which is particularly characterized by increased expression of SASPs (Takaya et al., 2023). These factors perturb the local microenvironment to induce chronic inflammation, which aggravates senescence (Wang et al., 2024). Therefore, strategies that can attenuate SASP-induced inflammation are of great therapeutic interest (Dash et al., 2025). Here, we found that vitisin B significantly reduced the expression of key SASP components, including IL-6, IL-8, IL-1β, and SAA1. These results were further supported by the finding that knockdown of *WBP2NL* gene, which was shown to be regulated by vitisin B, decreased the expression of key SASP components. Here, we propose the therapeutic potential of vitisin B in treating age-related inflammatory diseases by reducing the expression of key SASP components.

WBP2NL has a proline-rich WW domain that allows signaling

molecules to bind to the WW domain and initiate signal transduction (Marchak et al., 2017). Recent studies have found that *WBP2NL* expression is increased in breast cancer tissues, and acts as an anti-apoptotic factor that promotes breast cancer cell proliferation (Nourashrafeddin et al., 2015). However, no studies have investigated the effects of *WBP2NL* on senescence. In this study, we found that vitisin B down-regulated *WBP2NL* expression. Extending these results, down-regulating *WBP2NL* expression reduced mitochondrial ROS generation, similar to vitisin B treatment, thereby recovering senescence-associated phenotypes. These results suggest that the regulation of *WBP2NL* gene expression by vitisin B may be one of the potential ways to ameliorate senescence.

In summary, we discovered that vitisin B effectively reduced mitochondrial ROS in several PPs. The ROS-reducing effect of vitisin B is attributed to its ability to restore mitochondrial function, thereby efficiently transferring electrons in the ETC and recovering senescence-associated phenotypes. Moreover, we found that the senescence-ameliorating effect of vitisin B was accomplished by downregulation of *WBP2NL* expression. This mechanism is further supported by the result that *WBP2NL* knockdown induced a similar effect to vitisin B. These results point to a new way that vitisin B restores senescence by lowering ROS levels in the mitochondria. The anti-senescence mechanism of vitisin B will contribute to the development of new treatments for aging and age-related diseases.

CRediT authorship contribution statement

Ki Yong Lee: Writing – review & editing, Writing – original draft, Validation. **Jee Hee Yoon:** Writing – review & editing, Writing – original draft, Investigation, Conceptualization. **Youngjoo Byun:** Writing – review & editing, Writing – original draft. **Sekyung Oh:** Writing – review & editing, Writing – original draft, Investigation, Conceptualization. **Joon Tae Park:** Writing – review & editing, Writing – original draft, Supervision. **Yun Haeng Lee:** Writing – review & editing, Writing – original draft, Investigation, Conceptualization. **Hyung Wook Kwon:** Methodology, Investigation. **Minseon Kim:** Investigation. **Duyeol Kim:** Investigation. **Ji Ho Park:** Investigation. **Kyeong Seon Lee:** Investigation. **Byeonghyeon So:** Investigation. **Yoo Jin Lee:** Investigation.

Declaration of Competing Interest

The authors declare no conflicts of interest. The funders had no role in the collection, analyses, or interpretation of data; in the writing of the manuscript; or in the decision to publish the paper.

Acknowledgments

This research was supported by a grant of the Korea Health Technology R&D Project through the Korea Health Industry Development Institute (KHIDI), funded by the Ministry of Health & Welfare, Republic of Korea (RS-2023-KH140816, RS–2025–02303821) and the National Research Foundation of Korea grants funded by the Korean Government (NRF–2021R1A2C1093814).

Appendix A. Supporting information

Supplementary data associated with this article can be found in the online version at doi:10.1016/j.mad.2026.112159.

Data availability

Data will be made available on request.

References

Afzal, S., Abdul Manap, A.S., Attiq, A., Albokhadaim, I., Kandeel, M., Alhojaily, S.M., 2023. From imbalance to impairment: the central role of reactive oxygen species in oxidative stress-induced disorders and therapeutic exploration. Front Pharm. 14, 1269581.

Bjørkøy, G., Lamark, T., Pankiv, S., Øvervatn, A., Brech, A., Johansen, T., 2009. Monitoring autophagic degradation of p62/SQSTM1. Methods Enzym. 452, 181–197.

Brunk, U.T., Terman, A., 2002. Lipofuscin: mechanisms of age-related accumulation and influence on cell function. Free Radic. Biol. Med 33, 611–619.

Buffa, L., Saeed, A.M., Nawaz, Z., 2013. Molecular mechanism of WW-domain binding protein-2 coactivation function in estrogen receptor signaling. IUBMB Life 65, 76–84.

Checa, J., Aran, J.M., 2020. Reactive Oxygen Species: Drivers of Physiological and Pathological Processes. J. Inflamm. Res 13, 1057–1073.

Chen, Z.H., Lam, H.C., Jin, Y., Kim, H.P., Cao, J., Lee, S.J., Ifedigbo, E., Parameswaran, H., Ryter, S.W., Choi, A.M., 2010. Autophagy protein microtubule-associated protein 1 light chain-3B (LC3B) activates extrinsic apoptosis during cigarette smoke-induced emphysema. Proc. Natl. Acad. Sci. USA 107, 18880–18885.

Cho, H.-J., Hwang, J.-A., Yang, E.J., Kim, E.-C., Kim, J.-R., Kim, S.Y., Kim, Y.Z., Park, S. C., Lee, Y.-S., 2022. Nintedanib induces senolytic effect via STAT3 inhibition. Cell Death Dis. 13, 760.

Dan Dunn, J., Alvarez, L.A.J., Zhang, X., Soldati, T., 2015. Reactive oxygen species and mitochondria: A nexus of cellular homeostasis. Redox Biol. 6, 472–485.

Dash, U.C., Bhol, N.K., Swain, S.K., Samal, R.R., Nayak, P.K., Raina, V., Panda, S.K., Kerry, R.G., Duttaroy, A.K., Jena, A.B., 2025. Oxidative stress and inflammation in the pathogenesis of neurological disorders: Mechanisms and implications. Acta Pharm. Sin. B 15, 15–34.

Davan-Wetton, C.S.A., Montero-Melendez, T., 2024. An optimised protocol for the detection of lipofuscin, a versatile and quantifiable marker of cellular senescence. PLoS One 19, e0306275.

De Rossi, L., Rocchetti, G., Lucini, L., Rebecchi, A., 2025. Antimicrobial Potential of Polyphenols: Mechanisms of Action and Microbial Responses-A Narrative Review. Antioxid. (Basel) 14, 20.

Dickinson, B.C., Srikun, D., Chang, C.J., 2010. Mitochondrial-targeted fluorescent probes for reactive oxygen species. Curr. Opin. Chem. Biol. 14, 50–56.

Ebert, R., Benisch, P., Krug, M., Zeck, S., Meißner-Weigl, J., Steinert, A., Rauner, M., Hofbauer, L., Jakob, F., 2015. Acute phase serum amyloid A induces proinflammatory cytokines and mineralization via toll-like receptor 4 in mesenchymal stem cells. Stem Cell Res. 15, 231–239.

Fabris, S., Momo, F., Ravagnan, G., Stevanato, R., 2008. Antioxidant properties of resveratrol and piceid on lipid peroxidation in micelles and monolamellar liposomes. Biophys. Chem. 135, 76–83.

Gilbreath, C., Ma, S., Yu, L., Sonavane, R., Roggero, C.M., Devineni, A., Mauck, R., Desai, N.B., Bagrodia, A., Kittler, R., Raj, G.V., Yin, Y., 2021. Dynamic differences between DNA damage repair responses in primary tumors and cell lines. Transl. Oncol. 14, 100898.

González-Gualda, E., Baker, A.G., Fruk, L., Muñoz-Espín, D., 2021. A guide to assessing cellular senescence in vitro and in vivo. FEBS J. 288, 56–80.

Henderson, L.M., Chappell, J.B., 1993. Dihydrorhodamine 123: a fluorescent probe for superoxide generation? Eur. J. Biochem 217, 973–980.

Herb, M., Gluschko, A., Schramm, M., 2021. Reactive Oxygen Species: Not Omnipresent but Important in Many Locations. Front Cell Dev. Biol. 9, 716406.

Huang, L.C., Lin, W., Yagami, M., Tseng, D., Miyashita-Lin, E., Singh, N., Lin, A., Shih, S. J., 2010. Validation of cell density and viability assays using Cedex automated cell counter. Biologicals 38, 393–400.

Huang, W., Hickson, L.J., Eirin, A., Kirkland, J.L., Lerman, L.O., 2022. Cellular senescence: the good, the bad and the unknown. Nat. Rev. Nephrol. 18, 611–627.

Ichimura, H., Parthasarathi, K., Quadri, S., Issekutz, A.C., Bhattacharya, J., 2003. Mechano-oxidative coupling by mitochondria induces proinflammatory responses in lung venular capillaries. J. Clin. Invest 111, 691–699.

Ilie, O.-D., Ciobica, A., Riga, S., Dhunna, N., McKenna, J., Mavroudis, I., Doroftei, B., Ciobanu, A.-M., Riga, D., 2020. Mini-Review on Lipofuscin and Aging: Focusing on The Molecular Interface, The Biological Recycling Mechanism, Oxidative Stress, and The Gut-Brain Axis Functionality. Medicina 56, 626.

Kang, H.T., Park, J.T., Choi, K., Kim, Y., Choi, H.J.C., Jung, C.W., Lee, Y.-S., Chul Park, S., 2017. Chemical screening identifies ATM as a target for alleviating senescence. Nat. Chem. Biol. 13, 616–623.

Kauffman, M.E., Kauffman, M.K., Traore, K., Zhu, H., Trush, M.A., Jia, Z., Li, Y.R., 2016. MitoSOX-Based Flow Cytometry for Detecting Mitochondrial ROS. React. Oxyg. Species (Apex) 2, 361–370.

Kim, J.W., Kuk, M.U., Choy, H.E., Park, S.C., Park, J.T., 2019. Mitochondrial metabolic reprograming via BRAF inhibition ameliorates senescence. Exp. Gerontol. 126, 110691.

Kim, Y.H., Lee, Y.K., Park, S.S., Park, S.H., Eom, S.Y., Lee, Y.S., Lee, W.J., Jang, J., Seo, D., Kang, H.Y., Kim, J.C., Lim, S.B., Yoon, G., Kim, H.S., Kim, J.H., Park, T.J., 2023b. Mid-old cells are a potential target for anti-aging interventions in the elderly. Nat. Commun. 14, 7619.

Kim, Y.H., Lee, Y.-K., Park, S.S., Park, S.H., Eom, S.Y., Lee, Y.-S., Lee, W.J., Jang, J., Seo, D., Kang, H.Y., Kim, J.C., Lim, S.B., Yoon, G., Kim, H.S., Kim, J.-H., Park, T.J., 2023a. Mid-old cells are a potential target for anti-aging interventions in the elderly. Nat. Commun. 14, 7619.

Korkina, L.G., 2007. Phenylpropanoids as naturally occurring antioxidants: from plant defense to human health. Cell Mol Biol (Noisylegrand) 53, 15–25.

Kuk, M.U., Lee, H., Song, E.S., Lee, Y.H., Park, J.Y., Jeong, S., Kwon, H.W., Byun, Y., Park, S.C., Park, J.T., 2023. Functional restoration of lysosomes and mitochondria through modulation of AKT activity ameliorates senescence. Exp. Gerontol. 173, 112091.
Lee, H.C., Yin, P.H., Chi, C.W., Wei, Y.H., 2002. Increase in mitochondrial mass in human fibroblasts under oxidative stress and during replicative cell senescence. J. Biomed. Sci. 9, 517–526.
Lee, Y.H., Park, J.Y., Lee, H., Song, E.S., Kuk, M.U., Joo, J., Oh, S., Kwon, H.W., Park, J. T., Park, S.C., 2021. Targeting Mitochondrial Metabolism as a Strategy to Treat Senescence. Cells 10, 3003.
Lee, Y.H., Choi, D., Jang, G., Park, J.Y., Song, E.S., Lee, H., Kuk, M.U., Joo, J., Ahn, S.K., Byun, Y., Park, J.T., 2022. Targeting regulation of ATP synthase 5 alpha/beta dimerization alleviates senescence. Aging (Albany NY) 14, 678–707.
Lee, Y.H., Kuk, M.U., So, M.K., Song, E.S., Lee, H., Ahn, S.K., Kwon, H.W., Park, J.T., Park, S.C., 2023. Targeting Mitochondrial Oxidative Stress as a Strategy to Treat Aging and Age-Related Diseases. Antioxid. (Basel) 12, 934.
Lee, Y.H., So, B.H., Lee, K.S., Kuk, M.U., Park, J.H., Yoon, J.H., Lee, Y.J., Kim, D.Y., Kim, M.S., Kwon, H.W., Byun, Y., Lee, K.Y., Park, J.T., 2024. Identification of Cellular Isoschaftoside-Mediated Anti-Senescence Mechanism in RAC2 and LINC00294. Molecules 29, 4182.
Marchak, A., Grant, P.A., Neilson, K.M., Datta Majumdar, H., Yaklichkin, S., Johnson, D., Moody, S.A., 2017. Wbp2nl has a developmental role in establishing neural and non-neural ectodermal fates. Dev. Biol. 429, 213–224.
Mauthe, M., Orhon, I., Rocchi, C., Zhou, X., Luhr, M., Hijlkema, K.J., Coppes, R.P., Engedal, N., Mari, M., Reggiori, F., 2018. Chloroquine inhibits autophagic flux by decreasing autophagosome-lysosome fusion. Autophagy 14, 1435–1455.
Mitchell, P., Moyle, J., 1967. Chemiosmotic hypothesis of oxidative phosphorylation. Nature 213, 137–139.
Mizushima, N., Yoshimori, T., 2007. How to interpret LC3 immunoblotting. Autophagy 3, 542–545.
Mookerjee, S.A., Gerencser, A.A., Nicholls, D.G., Brand, M.D., 2017. Quantifying intracellular rates of glycolytic and oxidative ATP production and consumption using extracellular flux measurements. J. Biol. Chem. 292, 7189–7207.
Mottaghipisheh, J., 2021. Oxypeucedanin: Chemotaxonomy, Isolation, and Bioactivities. Plants (Basel) 10, 1577.
Naik, E., Dixit, V.M., 2011. Mitochondrial reactive oxygen species drive proinflammatory cytokine production. J. Exp. Med. 208, 417–420.
Nakai, K., Tsuruta, D., 2021. What Are Reactive Oxygen Species, Free Radicals, and Oxidative Stress in Skin Diseases? Int J. Mol. Sci. 22, 10799.
Neelam, Khatkar, A., Sharma, K.K., 2020. Phenylpropanoids and its derivatives: biological activities and its role in food, pharmaceutical and cosmetic industries. Crit. Rev. Food Sci. Nutr. 60, 2655–2675.
Nelson, G., Kucheryavenko, O., Wordsworth, J., von Zglinicki, T., 2018. The senescent bystander effect is caused by ROS-activated NF-κB signalling. Mech. Ageing Dev. 170, 30–36.
Nguyen, H.V.L., Grabow, J.-U., 2020. The Scent of Maibowle – π Electron Localization in Coumarin from Its Microwave-Determined Structure. ChemPhysChem 21, 1243–1248.
Nolfi-Donegan, D., Braganza, A., Shiva, S., 2020. Mitochondrial electron transport chain: Oxidative phosphorylation, oxidant production, and methods of measurement. Redox Biol. 37, 101674.
Nourashrafeddin, S., Aarabi, M., Modarressi, M.H., Rahmati, M., Nouri, M., 2015. The Evaluation of WBP2NL-Related Genes Expression in Breast Cancer. Pathol. Oncol. Res 21, 293–300.
Oh, K.-E., Shin, H., Lee, M.K., Park, B., Lee, K.Y., 2021. Characterization and Optimization of the Tyrosinase Inhibitory Activity of Vitis amurensis Root Using LC-Q-TOF-MS Coupled with a Bioassay and Response Surface Methodology. Molecules 26, 446.
Park, J.H., Jeong, E.Y., Kim, Y.H., Cha, S.Y., Kim, H.Y., Nam, Y.K., Park, J.S., Kim, S.Y., Lee, Y.J., Yoon, J.H., So, B., Kim, D., Kim, M., Byun, Y., Lee, Y.H., Shin, S.S., Park, J. T., 2025. Epigallocatechin Gallate in Camellia sinensis Ameliorates Skin Aging by Reducing Mitochondrial ROS Production. Pharmaceuticals 18, 612.
Park, J.Y., Lee, H., Song, E.S., Lee, Y.H., Kuk, M.U., Ko, G., Kwon, H.W., Byun, Y., Park, J. T., 2022. Restoration of Lysosomal and Mitochondrial Function Through p38 Mitogen-Activated Protein Kinase Inhibition Ameliorates Senescence. Rejuvenation Res. 25, 291–299.
Passos, J.F., Saretzki, G., Ahmed, S., Nelson, G., Richter, T., Peters, H., Wappler, I., Birket, M.J., Harold, G., Schaeuble, K., Birch-Machin, M.A., Kirkwood, T.B., von Zglinicki, T., 2007. Mitochondrial dysfunction accounts for the stochastic heterogeneity in telomere-dependent senescence. PLoS Biol. 5, e110.
Picca, A., Faitg, J., Auwerx, J., Ferrucci, L., D'Amico, D., 2023. Mitophagy in human health, ageing and disease. Nat. Metab. 5, 2047–2061.
Piipponen, M., Li, D., Landén, N.X., 2020. The Immune Functions of Keratinocytes in Skin Wound Healing. Int J. Mol. Sci. 21, 8790.
Pittayapruek, P., Meephansan, J., Prapapan, O., Komine, M., Ohtsuki, M., 2016. Role of Matrix Metalloproteinases in Photoaging and Photocarcinogenesis. Int J. Mol. Sci. 17, 868.
Plitzko, B., Loesgen, S., 2018. Measurement of Oxygen Consumption Rate (OCR) and Extracellular Acidification Rate (ECAR) in Culture Cells for Assessment of the Energy Metabolism. Bio Protoc. 8, e2850.
Poivre, M., Duez, P., 2017. Biological activity and toxicity of the Chinese herb Magnolia officinalis Rehder & E. Wilson (Houpo) and its constituents. J. Zhejiang Univ. Sci. B 18, 194–214.
Quan, T., Fisher, G.J., 2015. Role of Age-Associated Alterations of the Dermal Extracellular Matrix Microenvironment in Human Skin Aging: A Mini-Review. Gerontology 61, 427–434.
Rossi, M., Caruso, F., Antonioletti, R., Viglianti, A., Traversi, G., Leone, S., Basso, E., Cozzi, R., 2013. Scavenging of hydroxyl radical by resveratrol and related natural stilbenes after hydrogen peroxide attack on DNA. Chem. Biol. Interact. 206, 175–185.
Semple, F., Dorin, J.R., 2012. β-Defensins: Multifunctional Modulators of Infection, Inflammation and More? J. Innate Immun. 4, 337–348.
Sherratt, H.S., 1991. Mitochondria: structure and function. Rev. Neurol. 147, 417–430.
Stout, R., Birch-Machin, M.A., 2019. Mitochondria's Role in Skin Ageing. Biology 8, 29.
Sy, B., Krisa, S., Richard, T., Courtois, A., 2023. Resveratrol, ε-Viniferin, and Vitisin B from Vine: Comparison of Their In Vitro Antioxidant Activities and Study of Their Interactions. Molecules 28, 7521.
Takaya, K., Asou, T., Kishi, K., 2023. Cistanche deserticola Polysaccharide Reduces Inflammation and Aging Phenotypes in the Dermal Fibroblasts through the Activation of the NRF2/HO-1 Pathway. Int J. Mol. Sci. 24, 15704.
Tirichen, H., Yaigoub, H., Xu, W., Wu, C., Li, R., Li, Y., 2021. Mitochondrial Reactive Oxygen Species and Their Contribution in Chronic Kidney Disease Progression Through Oxidative Stress. Front Physiol. 12, 627837.
Turrens, J.F., 2003. Mitochondrial formation of reactive oxygen species. J. Physiol. 552, 335–344.
Ullah, A., Chen, Y., Singla, R.K., Cao, D., Shen, B., 2024. Pro-inflammatory cytokines and CXC chemokines as game-changer in age-associated prostate cancer and ovarian cancer: Insights from preclinical and clinical studies' outcomes. Pharmacol. Res. 204, 107213.
Vinh, L.B., Han, Y.K., Park, S.Y., Kim, Y.J., Phong, N.V., Kim, E., Ahn, B.-g, Jung, Y.W., Byun, Y., Jeon, Y.H., Lee, K.Y., 2023. Identification of triterpenoid saponin inhibitors of interleukin (IL)-33 signaling from the roots of Astragalus membranaceus. J. Funct. Foods 101, 105418.
Wang, J., Zhao, F., Xu, L., Wang, J., Zhai, J., Ren, L., Zhu, G., 2023. C-C Motif Chemokine Ligand 5 (CCL5) Promotes Irradiation-Evoked Osteoclastogenesis. Int J. Mol. Sci. 24, 16168.
Wang, Y., Li, Z., Xu, X., Li, X., Huang, R., Wu, G., 2024. Construction and validation of a senescence-related gene signature for early prediction and treatment of osteoarthritis based on bioinformatics analysis. Sci. Rep. 14, 31862.
Wei, Y., Ito, Y., 2006. Preparative isolation of imperatorin, oxypeucedanin and isoimperatorin from traditional Chinese herb "bai zhi"Angelica dahurica (Fisch. ex Hoffm) Benth. et Hook using multidimensional high-speed counter-current chromatography. J. Chromatogr. A 1115, 112–117.
Wu, M.F., Liao, C.Y., Wang, L.Y., Chang, J.T., 2017. The role of Slit-Robo signaling in the regulation of tissue barriers. Tissue Barriers 5, e1331155.
Xiao, J., 2017. Dietary flavonoid aglycones and their glycosides: Which show better biological significance? Crit. Rev. Food Sci. Nutr. 57, 1874–1905.
Yan, X., Yu, A., Zheng, H., Wang, S., He, Y., Wang, L., 2019. Calycosin-7-O-β-D-glucoside Attenuates OGD/R-Induced Damage by Preventing Oxidative Stress and Neuronal Apoptosis via the SIRT1/FOXO1/PGC-1α Pathway in HT22 Cells. Neural Plast. 2019, 8798069.
Yoon, J.E., Kim, Y., Kwon, S., Kim, M., Kim, Y.H., Kim, J.H., Park, T.J., Kang, H.Y., 2018. Senescent fibroblasts drive ageing pigmentation: A potential therapeutic target for senile lentigo. Theranostics 8, 4620–4632.
Yoon, J.H., Kim, Y.H., Jeong, E.Y., Lee, Y.H., Byun, Y., Shin, S.S., Park, J.T., 2024. Senescence Rejuvenation through Reduction in Mitochondrial Reactive Oxygen Species Generation by Polygonum cuspidatum Extract: In Vitro Evidence. Antioxidants 13, 1110.
Zhang, J., 2013. Autophagy and mitophagy in cellular damage control. Redox Biol. 1, 19–23.
Zhao, R.Z., Jiang, S., Zhang, L., Yu, Z.B., 2019. Mitochondrial electron transport chain, ROS generation and uncoupling (Review). Int J. Mol. Med 44, 3–15.